JAST. Vol. 9, No. 1, pp 13-26

JAST
Journal of Aerospace Science and Technology

An Innovation in Film Cooling of Gas Turbine Blades Applying an Upstream Jet

M.R. Salimi[1], M. Taeibi-Rahni[2], M. Ramezanizadeh[3], and R. Farhadi-Azar[4]

A new design concept is introduced to control the near-wall integration between the hot-gas boundary layer and the cooling jets in order to enhance the adiabatic film cooling effectiveness of the gas turbine blades. In this new approach, another film cooling port, having a very low blowing ratio, which prevents formation of the counter-rotating vortex pare, is applied just upstream of the main film cooling jet. The fluid injected from the small upstream port changes the flow pattern, results in wider horseshoe vortices in the span-wise direction, and generates a more uniform distribution of the coolant film. Also, this coolant fluid flows towards the low pressure region located just behind the main film-cooling hole. Therefore, by producing a cold layer of gas beneath the coolant jet and diverting the hot cross-flow gases into this area, it significantly improves the film cooling effectiveness, especially in the near field of the main jet. The obtained results show lower stream-wise velocity gradients near the wall, which considerably decreases the wall shear stresses, comparing to the regular film cooling holes. The investigations are performed using the Reynolds-averaged Navier-Stokes equations closed by the v^2f-kw turbulence model. The jet-to-cross flow velocity ratio and the main jet Reynolds number were 0.5 and 4700, respectively.

***Keywords**: Innovation in Film Cooling, Gas Turbine Blades, Upstream Jet, Numerical Simulation, v^2f-kw Turbulence Model*

Nomenclature

k	Turbulence Kinetic Energy	P_k	Turbulence Production
ε	Turbulence Dissipation Rate	T	Temperature
ω	Specific Dissipation Rate	L	Turbulence Length Scale
v^2	Normal to Streamline Component of Reynolds Stress Tensor	v_t	Turbulence Viscosity
f	Elliptic Relaxations Parameter	U_i	Mean Flow Velocity Vector
$\overline{u'_i u'_J}$	Reynolds Stress Tensor	ρ	Flow Density
$\overline{T'u'_j}$	Specific Turbulent Heat Flux	S_{ij}	Strain Rate Tensor
Re_y	Wall Reynolds Number	D_j	Jet Width
V_{cf}	Mean Cross Flow Velocity	M_{in}	Inlet Mass Flow Rate
AR	Upstream to Main Jet Area Ratio	M_{out}	Outlet Mass Flow Rate
T	Time	t_l	Turbulence Time Scale

1 Introduction

The desire for higher specific thrust in air, land and sea gas turbines renders the need for high temperature rise combustors, and this, in turn, implies increases in turbine entry temperatures [1]. However, these high, operative temperatures affect the durability of the blade. To prevent damaging of the blades, a variety of cooling techniques has been developed. These techniques fall into two major categories: internal and external cooling. Both techniques use cold air extracted from the compressor section and pass it through channels within the blade (internal cooling), where tabulators such as ribs and pin fins are used to increase the rate of heat removal

1. Ph.D Student, Dep't. of Aerospace Eng., Sharif University of Technology, Tehran, Iran. Email address: salimi1362@gmail.com
2. Professor, Dep't. of Aerospace Eng., Sharif University of Technology, Tehran, Iran.
3. Assistant Professor (Corresponding Author), Dep't. of Aerospace Eng., Shahid Sattari Aeronautical University of Science & Technology, Tehran, Iran. Email address: ramezanizadeh@gmail.com
4. M.Sc. Graduate, Dep't. of Aerospace Eng., Sharif University of Technology, Tehran, Iran.

sufficient to maintain the blade at the required temperatures and although transpiration may be required in the future, problems associated with the blade strength and the dimensions of the pores remain to be solved. Thus, film cooling is required and usually takes the form of rows of discrete holes along the span of the blades. In film cooling, the coolant forms a film layer over the blade surface to protect it from direct exposure to the hot gas stream. Due to the interactions between the coolant jets and the surrounding laminar or turbulent boundary layer around the blades, the flow in the vicinity of the discharge holes is particularly complex. The flow patterns are characterized by the development of a horseshoe-like vortex wrapped around the jet exit and a counter-rotating vortex pair (CRVP), which is formed as the jet enters the cross-flow and dominates the far field [3].

Since 1950, many researchers have studied this problem and observed many physical and geometrical parameters affecting the film cooling effectiveness. Some of the most important ones are discussed here. Altorairi [4] investigated the effects of creating a trench about a row of film cooling holes. The results of this study confirmed that trench could improve adiabatic effectiveness due to increasing lateral spreading and reducing coolant jet separation. Also, Baheri et al. [5] showed that the trenched-shaped holes could increase the film cooling effectiveness rather than simple trenched holes. The length-to-diameter ratio of the trenched holes was found to have a significant effect on film cooling effectiveness and on the spread of the coolant jets. Waye and Bogard [6] examined nine trench configurations on the suction side of a turbine vane experimentally. They showed that the perpendicular trench wall near the downstream edge of the coolant hole improves the adiabatic effectiveness rather than other configurations.

Ramezanizadeh et al. [7] studied the effects of density ratio in the film cooling flow hydrodynamics by using the LES approach. They observed that variation of jet to cross flow temperature ratio, which results in non-unity density ratios, significantly affects the expansion and the location of the CRVP and that of the horseshoe vortices (HSVs). For instance, the CRVP's position moves far away from the wall and the jet gradually becomes separated from the surface as the density ratio increases. They also reported that this condition causes the film cooling effectiveness to reduce, as the density ratio increases.

Dittmar et al. [8], Miao and Wu [9], and Lu et al. [10] showed that the vertical flow generated downstream of the jet and the interaction between the coolant jet and the hot cross flow are severely affected by the jet hole shape. For instance, using shower head or fan-shaped holes has superior effects on the film cooling effectiveness.

Yuen and Botas [11] and Goldstein et al. [12] investigated the film cooling characteristics of a single round hole jet injected at various stream-wise angles of $30^\circ, 60^\circ, 90^\circ$ into the cross flow. Their results showed that, for blowing ratios of 0.5 and 0.67, maximum effectiveness is achieved by the 30° hole. For steeper (60° and 90°) holes, penetration of the coolant jets into a hot cross flow boundary layer and the flow separation is higher. Therefore, relatively lower values of stream-wise angles are more suitable in practical situations.

Nasir et al. [13] studied the effects of the discrete triangular-shaped tabs with different orientations on the film cooling performance from a row of cylindrical holes. Tabs are placed along the upstream edge of the hole. Their results showed that the horizontal and downward-oriented tabs appear to exhibit the highest film cooling effectiveness and less pressure drop. They reported that this higher effectiveness is due to the generation of secondary eddies counter-rotating with respect to the CRVPs, which reduce the jet penetration and increase the film cooling effectiveness.

Rowbary and Oldfield [14] and Cutbirth and Bogard [15] investigated the effects of the cross flow turbulence intensity. They showed that the turbulence intensity considerably enhances the mixing of the coolant jet with the main hot cross flow at high blowing ratios, in which the coolant jet is detached from the surface. However, it has little effect on low blowing ratios, because of which the coolant jet remains attached to the surface.

Sangkwon and Shih [16] proposed placing an upstream ramp to modify the hot gas boundary layer/cooling jet interaction. The obtained results showed that the ramp, by deflecting the approaching boundary layer flow away from the base of the film cooling jet, causes lower boundary layer interaction between the jet and the cross flow. Taking the ramp further away from the surface eliminates the horseshoe vortices and allows the film jet to spread out more laterally. These flow features were found to improve the film cooling adiabatic effectiveness.

Javadi et al. [17] proposed placing two small injection ports just downstream of the film-cooling-hole exit, which produces vortices in the opposite direction of the main jet CRVP vortices and, therefore, reduces their strength. This approach provides considerable improvement in a) film cooling efficiency (at least 50% higher than in line arrangement), b) uniform distribution of the coolant film, and c) reduction of the skin friction drag.

Acharya et al. [18] studied the film cooling of a jet into a cross flow using different numerical approaches, namely direct numerical simulation (DNS), large eddy simulation (LES), and several different turbulence models including the k–ε and the Reynolds stress transport models (RSM). They reported that the two-equation models usually under-predict the lateral spreading of the film cooling jet and over-predict its vertical pen-

etration. Also, they did not find the RSTM predictions to be substantially better than the two-equation model predictions. However, LES and DNS results predicted the mean velocities and the turbulent stresses better.

Jones [19] investigated the film cooling problem using four different turbulence models, namely the $k-\varepsilon$, $k-\omega$, $v^2f-k\varepsilon$, and the $v^2f-k\omega$ (which is based on ω as the relevant length scale and provides predictive accuracy that is comparable to or better than $v^2f-k\varepsilon$ having significantly improved numerical stability). They reported that the $v^2f-k\omega$ model provides improved flow prediction over other turbulence models. Also, they proposed a new prandtl number expression which yields improved cooling effectiveness predictions.

So far, many studies have been conducted to understand the physical phenomena regarding the film cooling problem. They tried to improve the surface protection using minimum amount of coolant fluid. In this work, a new approach is introduced to modify the hot gas boundary-layer/cooling jet interaction so that the film-cooling effectiveness and its distribution may improve. In this new innovation, an upstream injection port (Fig.2) is proposed. Using this new approach, the following advantages will be archived:

1. Increasing the film cooling effectiveness,
2. Enhancing the uniformity of the film-cooling effectiveness distribution, and
3. Reducing skin friction drag.

Note that, contrary to the previous works, the film-cooling effectiveness was improved using relatively simple hole geometry (squared) and injection angle (90 deg). Also, the $v^2f-k\omega$ turbulence model is applied to provide more accurate flow prediction and less numerical instability, in comparison to the relevant two-equation models.

2 Governing Equations

The governing equations are the steady state incompressible continuity, momentum, and energy equations. The fluid properties are assumed constant, which is a reasonable assumption compared to the corresponding experiments. Using the Reynolds averaged Navier-Stokes approach, we have:

$$\frac{\partial U_i}{\partial x_i}=0, \tag{1}$$

$$\frac{\partial\left(U_iU_j\right)}{\partial x_j}=-\frac{1}{\rho}\left(\frac{\partial p}{\partial x_i}\right)+\frac{\partial}{\partial x_j}\left(2\upsilon S_j-\overline{u_i'u_j'}\right), \tag{2}$$

$$\frac{\partial\left(U_iT\right)}{\partial x_j}=\frac{\partial}{\partial x_j}\left(\frac{\upsilon}{pr}\frac{\partial T}{\partial x_j}-\overline{T'u_j'}\right), \tag{3}$$

where $-\overline{u_i'u_j'}$ is known as the specific Reynolds stress tensor, and $c_p\overline{T'u_j'}$ are the specific turbulent heat fluxes. Both of these terms need to be modeled, which is known as the closure problem of the turbulence. Three different turbulence models including the $k-\omega$ (Wilcox), SST (Menter), and $v^2f-k\omega$ are applied here.

3 Turbulence Models

Considering the poor numerical convergence behavior of the $v^2f-k\varepsilon$ model, Jones developed a new model, namely the $v^2f-k\omega$ model [19]. This new model does not suffer from the numerical stiffness of the $v^2f-k\varepsilon$ model, but shows improved predictions similar to that of the $v^2f-k\varepsilon$ model. The basic philosophy in developing this new model lies in introducing a new $\varepsilon-\omega$ relationship (instead of $\varepsilon=\beta^*\omega k$ which is used in the standard $k-\omega$ model) that is based not only on dimensional arguments, but also on the need for preserving the v^2k/ε scaling in the eddy-viscosity expression. The following equation is proposed to relate ε and ω:

$$\varepsilon=func\left[\beta^*\omega k^n\overline{v^2}^{1-n}\right]+\left(1-func\right)\frac{2\upsilon k}{y^2}. \tag{4}$$

where $n=0.7$, and y represents the wall normal distance. Also,

$$func=[1-\exp(-0.02\,\mathrm{Re_y})]^2 \tag{5}$$

in which,

$$\mathrm{Re_y}=\frac{\sqrt{k}\,y}{\upsilon}. \tag{6}$$

The relationship between ε and ω, which is proposed in equation (4), has been shown by Jones to provide the best fit to eddy viscosity computed on the basis of the DNS data. The second part of equation (4) is introduced to provide the physically correct asymptotic behavior of eddy viscosity for flow in a channel, and also shows

good agreement with experiments for flow in a coaxial jet and flow over a heated cavity [20]. The resulting governing equations for the $v^2 f - k\omega$ model are:

$$\frac{\mathrm{D_k}}{\mathrm{D_t}} = P_k - \varepsilon + \frac{\partial}{\partial x_j}\left[(\upsilon + \upsilon_t)\frac{\partial k}{\partial x_j}\right], \tag{7}$$

$$\frac{D\omega}{Dt} = \alpha\frac{\omega}{k}P_k - \beta\omega^2\left(\frac{\overline{v^2}}{k}\right)^{1-n} + \frac{\partial}{\partial x_j}\left[(\upsilon + \sigma\upsilon_t)\frac{\partial \omega}{\partial x_j}\right], \tag{8}$$

$$\frac{D\overline{v^2}}{Dt} = kf - \varepsilon\frac{\overline{v^2}}{k} + \frac{\partial}{\partial x_j}\left[(\upsilon + \upsilon_t)\frac{\partial \overline{v^2}}{\partial x_j}\right], \tag{9}$$

$$L^2\nabla^2 f - f = \frac{C_1}{t_l}\left(\frac{\overline{v^2}}{k} - \frac{2}{3}\right) + C_2\frac{P_k}{k}. \tag{10}$$

where, P_k, t_l and L define the turbulence production, time and length scales respectively. They are computed as follow:

$$P_k = 2\upsilon_t S_j \frac{\partial u_i}{\partial x_j}, \tag{11}$$

$$t_l = \min\left\{\max\left(\frac{k}{\varepsilon}; 6\sqrt{\frac{\upsilon}{\varepsilon}}\right); \frac{\alpha k}{\sqrt{6}\overline{v^2}C_\mu|S|}\right\}, \tag{12}$$

$$L = C_l \max\left\{\min\left(\frac{k^{3/2}}{\varepsilon}; \frac{k^{3/2}}{\sqrt{6}C_\mu\overline{v^2}|S|}\right); C_\eta\left(\frac{\upsilon^3}{\varepsilon}\right)^{1/4}\right\}, \tag{13}$$

in which, $|S|$ is the magnitude of the strain rate tensor. The eddy viscosity and other coefficients are defined as

$$\upsilon_t = C_\mu \overline{v^2} t_l. \tag{14}$$

$$\beta^* = 0.09, \quad \beta = \frac{4}{5}\beta^*, \quad C_1 = 0.4, \quad C_2 = 0.3, \quad \sigma_{\omega^*} = 1.5,$$

$$\alpha = \frac{\beta}{\beta^*} - \frac{1}{\sigma_\omega}\left[\kappa^2/\sqrt{\beta^*}\right], \quad C_L = 0.23, \quad C_\mu = 0.25, \quad \kappa = 0.41.$$

Ignoring the details, the turbulence models adopted in this study also include the standard and the shear-stress transport (SST) $k-\omega$ models. The standard $k-\omega$ model is an empirical model based on a transport equation for the turbulent kinetic energy (k) and a specific dissipation rate (ω), which can also be considered as the ratio of ε and k. The low Reynolds number effect is accounted for in the $k-\omega$ model [21, 22]. The SST model is a mixture of the $k-\omega$ and the $k-\varepsilon$ models. That is, close to the wall, it becomes the $k-\omega$ model, while in the far field, the $k-\varepsilon$ model is applied [23].

4 Numerical Approaches

Solutions to the aforementioned governing equations were obtained using the finite volume method and the steady SIMPLE algorithm. The numerical code which is developed by the authors uses a staggered mesh arrangement and employs the Power-Law scheme to calculate the fluxes at the control-volume faces. A tri-diagonal matrix algorithm (TDMA) is used to solve the equations. The under-relaxation coefficients applied for the momentum equations are 0.7 and for the turbulence equations are 0.6. The utilized grid points are 140×80×45 for the main flow, 16×32×16 for the main jet, and 8×32×16 for the upstream jet in x, y and z directions, respectively. In both cross flow and jet flow blocks, grid refinement near the solid walls was performed using the following algebraic stretching formula:

$$Y = H\frac{(\beta+1) - (\beta-1)\left\{\left[(\beta+1)/(\beta-1)\right]^{(1-\eta)}\right\}}{\left[(\beta+1)/(\beta-1)\right]^{(1-\eta)} + 1}, \tag{15}$$

where, η and β are the metric and the clustering coefficients, respectively. Also, grid refinement was performed in X- and Z-directions in the cross flow block. That is, the grid was stretched close to the jet exit and was expanded away from it.

5 Physical Domain and Boundary Conditions

Different physical domains based on the ordinary and new film-cooling approaches are considered. The applied boundary conditions include inlet, outlet, no flux, periodic, and solid wall.

5.1 Ordinary Film-Cooling Physical Domain

For the code validation purpose, the single jet results are compared with those of a square jet normally injected into a cross flow (Fig.1), which are the experimental (LDV) and numerical (standard $k-\varepsilon$) results of Ajersch et al [24]. Their jet hydraulic diameter (jet width D) was 12.7 mm and the jet Reynolds number (based on D) was 4700 with a uniform velocity of $5.5\,m/s$ at the entrance of the jet channel. It should be noted that; they used three velocity ratios of 0.5, 1.0, and 1.5, whereas, here, the simulations are performed at the velocity ratio of 0.5 (a more common value in film cooling applications). Here, the dimensionless jet channel's length was $5D$ and the cross-flow domain was extended from $5D$ upstream to 40D downstream (from the center of the jet cross section). Also, in the vertical direction, the domain was extended to 20D above the wall.

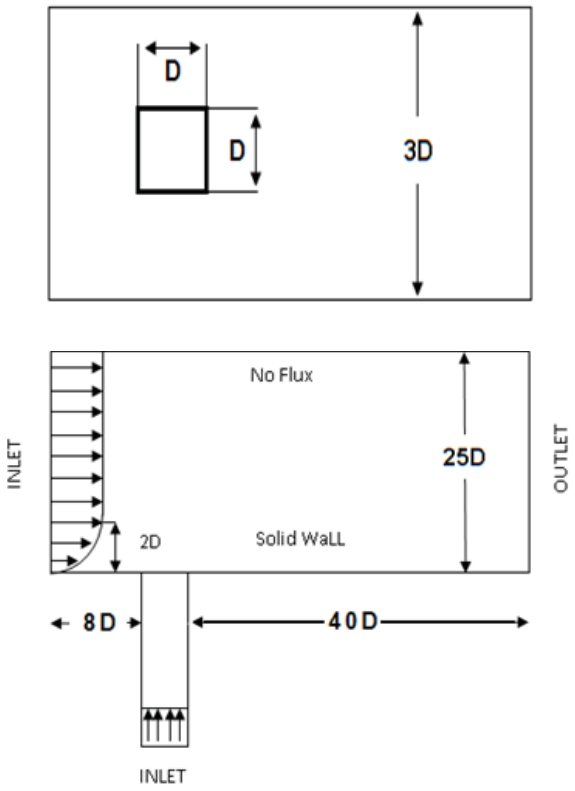

Figure 1. Physical domain of the ordinary film-cooling configuration [24].

5.2 Physical Domain of the New Film-Cooling Approach

In this work, a new design concept is introduced by placing another injection hole just upstream of the main cooling hole in order to modify the approaching boundary layer flow and its interaction with the film-cooling jet (Fig. 2). To be able to compare the results of this work with those of the ordinary approach, the same amount of total coolant air was used. Note that other parameters, such as the size of the physical domain and the jet Reynolds number, were taken to be the same as those of the ordinary film-cooling case. In order to prevent formation of CRVP for the upstream jet, its blowing ratio was kept too small (0.125).

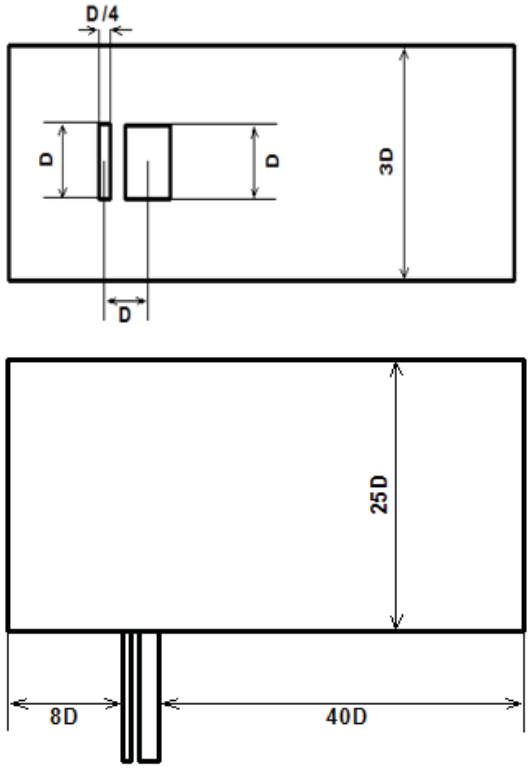

Figure 2. Physical domain of the new film-cooling configuration.

5.3 Boundary Conditions

Five different types of boundary conditions, namely inflow, outflow, no flux, solid wall, and periodic were used as follows:

a) *Inflow Boundary Condition:* At the inlet, the boundary layer thickness was set to $2D$ to match the benchmark data [24]. For the boundary layer at the inlet plane of the main flow, the one-seventh power law profile was used for the $x-$velocity component, whereas a

uniform stream-wise velocity was implemented above $Y = 2D$ and other velocity components were set to zero. The turbulent kinetic energy was taken from the experimental data of Ajersch et al. [24] where the inlet turbulence intensity was considered to be 1.2% for the main flow and the jet flow. Assuming isotropic flow at the jet and the cross flow entrance, the values of $\overline{v^2}$ were set to 2k/3 in these locations.

The inlet turbulent specific dissipation rate can be obtained from the following relation:

$$\omega_{in} = \frac{(1 \to 10)V_{cf}}{L}, \tag{16}$$

where L is the approximate length of the physical domain [24].

b) *Outflow Boundary Condition:* The gradient of the flow quantities was considered to be zero at the outflow boundary. Also, to ensure the conservation of mass, the following relation for the stream-wise velocity component was applied:

$$\overline{u}_{NI,J,k} = \overline{u}_{NI-1,J,k}\left(\dot{M}_{in} / \dot{M}_{out}\right), \tag{17}$$

where $\dot{M}_{in}$ and $\dot{M}_{out}$ are the inlet and outlet mass flow rates, respectively.

c) *No-flux Boundary Condition:* At the infinity (far from the wall), the no-flux boundary condition was used as follows:

$$\frac{\partial \varphi}{\partial n} = 0.0, \tag{18}$$

where n denotes the direction normal to the face.

d) *Periodic Boundary Condition:* It was assumed that there are several coolant jets in the span-wise direction. To consider the effects of the other jets, the periodic boundary condition was used as:

$$\varphi_{i,j,1} = \varphi_{i,j,NK-1}, \qquad \varphi_{i,j,NK} = \varphi_{i,j,2}. \tag{19}$$

e) *Solid-wall Boundary Condition: The n*o-slip and adiabatic-wall boundary conditions were used at the solid walls. Also, the wall boundary conditions for all of the turbulence model equations are:

$$k = 0.0, \qquad \text{all models}, \tag{20}$$

$$\overline{v^2} = 0.0, \qquad \text{for the } \overline{v^2} f - k\omega \text{ model}, \tag{21}$$

$$\omega_w = \frac{2\upsilon}{\beta^* y^2}\left(\frac{k}{\overline{v^2}}\right)^{1-n}, \qquad \text{for the } \overline{v^2} f - k\omega \text{ model}, \tag{22}$$

$$\omega_w = \frac{60\upsilon}{\beta_1 y^2}, \qquad \text{for the } SST \text{ model}, \tag{23}$$

$$\omega_w = \frac{60\upsilon}{\beta^* y^2}, \qquad \text{for the } k-\omega \text{ model}, \tag{24}$$

$$f_w = -\frac{20\upsilon^2 \overline{v^2}}{\varepsilon_w y^4}, \qquad \text{for the } \overline{v^2} f - k\omega \text{ model}, \tag{25}$$

where, y is the normal distance from the wall, υ is the molecular kinematics viscosity, and β_1, β^* are constants.

6 Grid-Sensitivity and Code-Validation Studies

The solution accuracy strongly depends upon the quality of the grid. The grid quality highly affects the grid induced error minimization and the ability to resolve the relevant flow physics. Here, the grid resolution study was performed applying four different grid arrangements. The total grid points used in each direction for the main flow, the main jet, and the smaller upstream jet are shown in Tables 1, 2, and 3, respectively. By grid refining, most of the cells were concentrated about the film cooling jet and the hot-gas/coolant-jet interaction region, in which the flow physics is more complicated (see Fig.3 for details of the grid spacing). The comparisons were performed using the centerline film cooling effectiveness. These comparisons are shown in Fig. 4. Based on these comparisons, the third grid was considered for the flow simulation.

Table 1. Number of grid points used in the main flow domain.

Case	Ni	Nj	Nk	Total
1	130	45	25	146250
2	130	70	25	227500
3	140	80	45	504000
4	160	100	60	960000

Table 2. Number of grid points used in the main jet channel.

Case	Ni	Nj	Nk	Total
1	12	20	10	2400
2	12	28	10	3360
3	16	32	16	8192
4	18	38	18	12312

Table 3. Number of grid points used in the upstream jet channel.

Case	Ni	Nj	Nk	Total
1	6	20	10	1200
2	6	28	10	1680
3	8	32	16	4096
4	10	38	18	6840

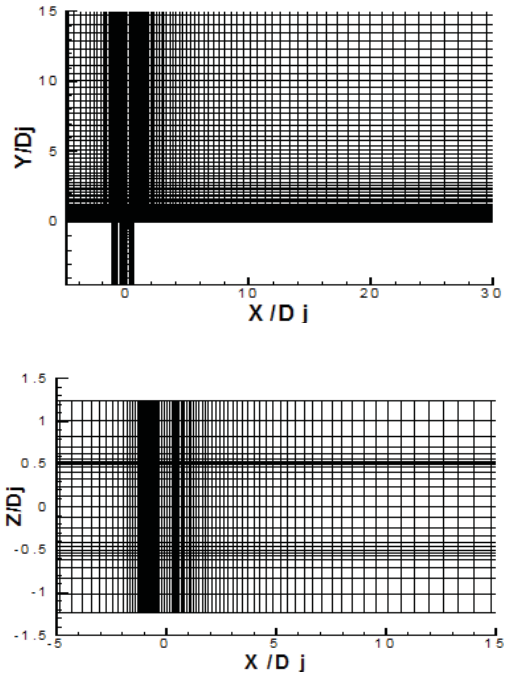

Figure 3. Grid used for the new film-cooling configuration.

-

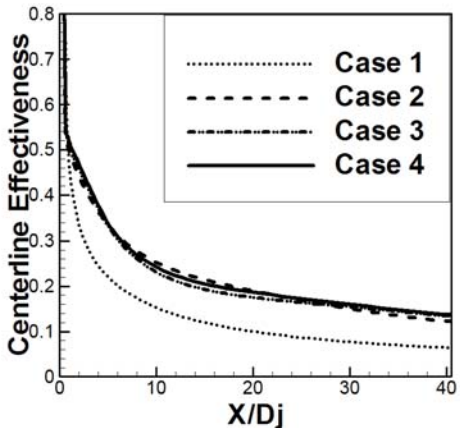

Figure 4. Grid resolution study on the profiles of centerline cooling effectiveness.

In order to validate the obtained results of the ordinary film cooling problem (single jet), the results were compared with those of the experimental data of Ajersch et al. [24]. As mentioned earlier, the jet-into-cross flow problem is a highly complex turbulent flow including acceleration/deceleration, wake, and highly swirling/rotating behavior with strong streamline curvature and backflow regions. All of these features introduce non-isotropic effects into the flow field and the two-equation turbulence models fail to simulate most of these phenomena's accurately (Jones et al. [19]).

Hence, the $\overline{v^2}f-k\omega$ turbulence model was applied which was shown to produce good results in simulating the film cooling problem.

The stream-wise velocity component prediction of each model at the span-wise center plane (Z/D_j=0) and the stream-wise location of X/D_j=5 is shown in Fig .5. As shown in this figure, the $k-\omega$ and SST models considerably over-predict the stream-wise velocity component close to the surface. Therefore, it is evident that they also over-predict the wall shear stress and drag coefficient due to higher near-wall velocity gradient as shown in Fig .5. On the contrary, the $\overline{v^2}f-k\omega$ results are in good agreement with those of the Ajersch et al. [24]. Based on this outcome and the fact that the $\overline{v^2}f-k\omega$ generates lower eddy viscosity near the wall [19-20], one can show that (Eq. 11) the turbulence production in the vicinity of wall and jet shear layers for the $\overline{v^2}f-k\omega$ model is higher than that of the $k-\omega$ and SST models.

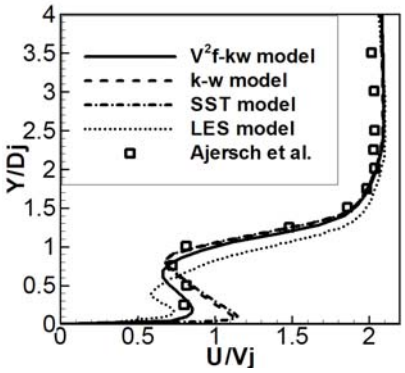

Figure 5. Comparison of the stream-wise velocity components provided by different turbulence models at Z/D=0.0 and X/D=5.0.

Figure 6 demonstrates the turbulence kinetic energy profiles at the jet center plane for X/D_j=3 , X/D_j=5 , and X/D_j=8. As shown in this figure, both the $k-\omega$ and the SST models under-predict the turbulence kinetic energy near the wall. The $v^2f-k\omega$ model predicts better kinetic energy near the wall, since a two layer approach is used to compute the k equation [19]. So, the $v^2f-k\omega$ shows improvement over the $k-\omega$ and the SST models, but it shows a slight over-prediction in the maximum value of the kinetic energy. This shows that the turbulence level predicted by the $v^2f-k\omega$ model in the vicinity of the wall and jet shear layers is higher than that of the $k-\omega$ and SST models. Therefore, based on the discussions presented in the previous paragraph, it is concluded that the $v^2f-k\omega$ model predicts a higher dissipation rate, in comparison to the $k-\omega$ and the SST models. Therefore, the turbulence kinetic energy over-prediction of the $v^2f-k\omega$ model in the jet shear layer seems to be due to excessive production of turbulence dissipation rate in this region.

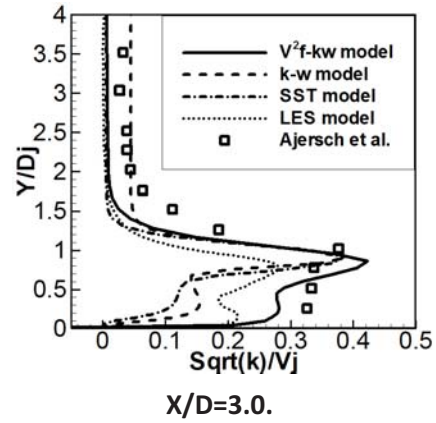

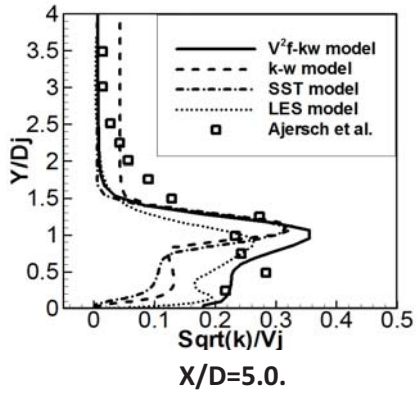

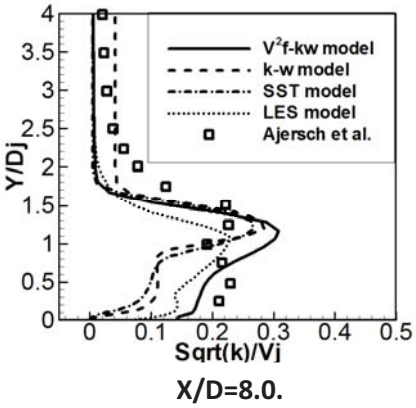

Figure 6. Comparison of turbulence kinetic energy profiles provided by different turbulence models at Z/D=0.0.

A new approach was introduced to control the near-wall interaction between the jet and the cross flow to improve the film cooling effectiveness and to reduce the skin friction drag. It is suggested to place another film cooling port (with a very low blowing ratio of 1.25) just upstream of the main jet. In this section, the hydrodynamic behavior of the flow induced by the upstream jet is described comparing to that of the single jet flow. Also, the effects of the upstream hot jet and the effects of the upstream to main jet width ratio on the flow characteristics are investigated. Finally, the effects of the upstream jet on the skin friction drag coefficient are investigated.

7.1 Hydrodynamics of the Flow

Generation of horseshoe vortices is due to the interactions between the jet and the main flow boundary layers, as the fluid in the main flow boundary layer is deflected laterally away from the center plane due to the adverse pressure gradient in front of the jet. The span-wise vorticity in the main flow boundary layer is stretched to form the front of the horseshoe vortices. These vortices are convected and tilted such that the two branches compose the characteristic horseshoe shape [24]. Note that these vortices separate the film cooling holes affected area from that of the hot cross flow gases in the near-field region of the jet.

The major physical differences between the new jets' configuration flow characteristics and those of the ordinary film cooling holes are discussed in the following four steps:

a) In the new configuration, as shown in Fig. 7, the static pressure upstream of each film cooling hole reduces (due to the flow separation in this region) and permits the flow from the main jets to move upward and make the recirculation flow in this region. Then, the vortices are convected downward by the cross flow and make the horseshoe vortices. However, the size of the recirculation region is comparable to the size of the upstream jet width and, hence, the horseshoe vortices of this flow are much wider (depending on the width of the upstream jet hole) in comparison to the ordinary film cooling flow (single jet). Wider HSV means more span-wise spreading of the coolant fluid, which results in more uniform film cooling distribution, especially in the near field region of the jet exit. This fact is evident from Fig. 8, in which the film cooling effectiveness contours of the upstream jet configuration are compared with those of the ordinary film cooling hole. In Fig. 9, the span-wise averaged effectiveness and the centerline film cooling effectiveness of the new configuration are compared with those of the ordinary jet. It could be observed that the new configuration improves the span-wise averaged effectiveness both in the near and far field of the flow, but the centerline effectiveness increases just in the near-field region and has no important effect on the far field region (due to more jet penetration).

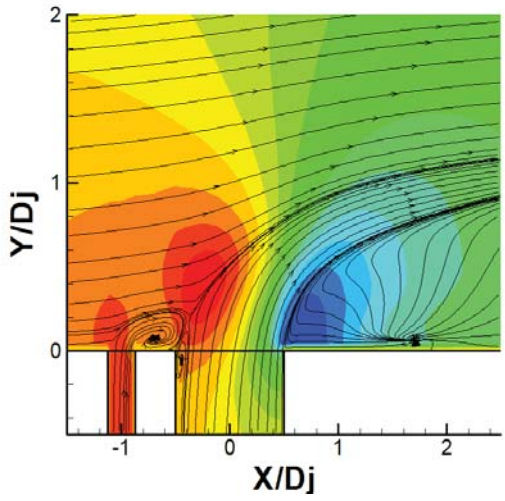

Figure 7. Stream lines and pressure contours at Z/D=0.0.

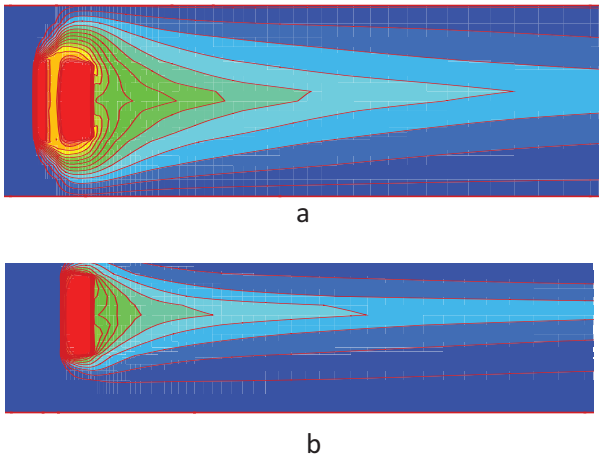

Figure 8. Film cooling effectiveness contours
a) new configuration b) ordinary jet configuration.

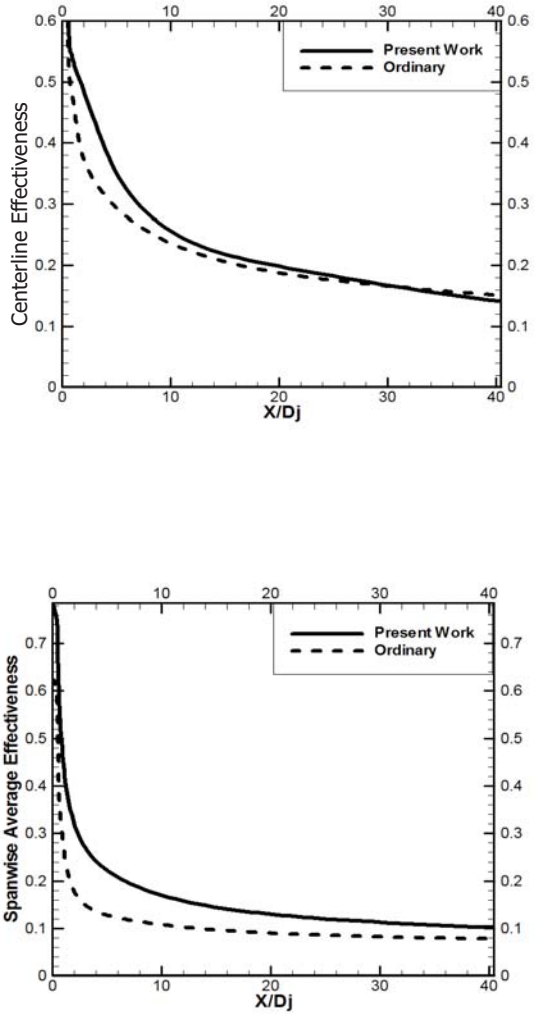

Figure 9. Comparison of the span-wise averaged and centerline film cooling effectiveness.

b) Injection of the coolant jets into the cross flow makes a low pressure region just behind the jets causing the hot gases to flow into this region, producing a layer of hot gases beneath the coolant jets, and thus, reduces the film cooling effectiveness. However, in the new approach, the coolant fluid of the upstream jet flows toward this region (due to the pressure difference) and prevents the hot gases from touching the surface. However, this effect is limited to the near field of the jets. As shown in Fig. 9, the difference between the two curves becomes less and less moving away from the jet exit. It shows that the near field of the jet is more affected in the new configuration.

c) When the upstream jet exists, the main jet is not deflected by the approaching boundary layer flow when it is fairly above the surface. Therefore, higher penetration of the jet into the cross flow boundary layer occurs in the new configuration. Figure 10 compares the stream-wise velocity profiles of the upstream jets' configuration with those of the ordinary jet at $Z/D_j = 0$ at the stream-wise location of X/D_j=10. As shown in this figure, for the new configuration, 1) The jet penetration is higher, 2) The velocity gradient near the wall is much lower, which is desirable from the skin friction drag reduction standpoint, and 3) The wake flow is weaker.

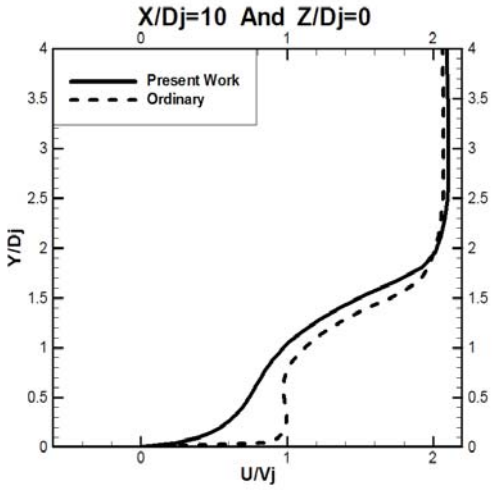

Figure 10. Comparison of stream-wise velocity profiles of the new configuration with the ordinary jet.

As mentioned in part **(c)**, for the new jet configuration, the main jet flow does not interact with the cross flow when it is fairly above the surface where its cross section area is higher and, hence, its effective blowing and momentum ratios are lower than those of the ordinary jet system. It is evident that lower momentum ratio means weaker CRVPs and, hence, less mixing occurs between the coolant jets and the hot cross flow. This is useful from the cooling performance point of view. Fig. 11 compares the span-wise velocity component profiles of the new configuration with those of the ordinary jet at Z/D_j=-0.5 and X/D_j=10 location. Note that in the new jet configuration, the peaks in the span-wise velocity component are lower than those of the ordinary jet. This means that the CRVPs of the new jet configuration are much smaller and, hence, weaker. Fig. 12 shows the local temperature distribution at different locations of X/D_j=3,5 downstream of the coolant jets for both the ordinary and the new film cooling configurations. This figure illustrates that the coolant film in the new configuration spreads

higher in both span-wise and normal directions.

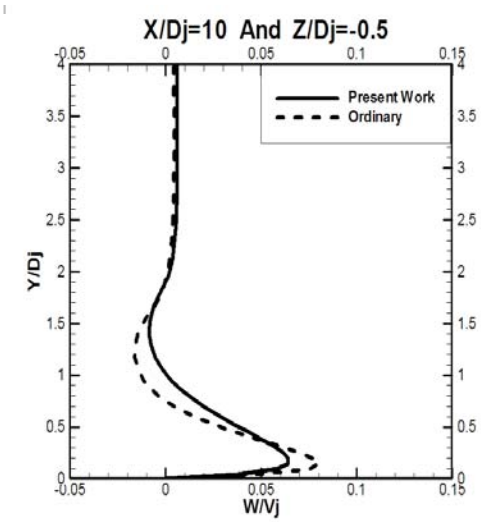

Figure 11. Comparison of the span-wise velocity profiles of the new configuration with those of the ordinary jet.

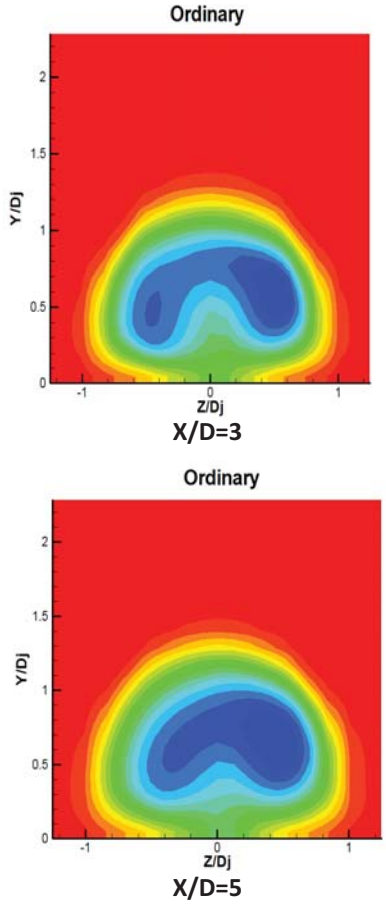

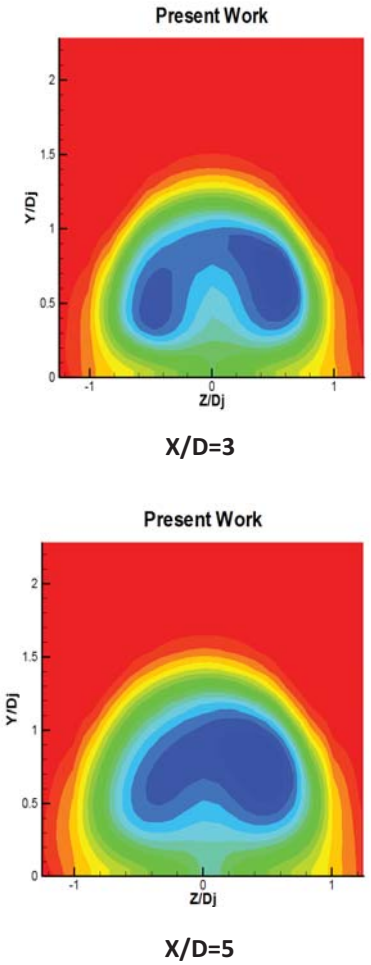

Figure 12. Local temperature distribution at different X/D positions.

7.2 Hot Upstream Jet

In the previous section, four major physical differences between the new jets' configuration flow characteristics and those of the ordinary film cooling holes were discussed. Three of them (parts a, b, and d) help to increase the cooling effectiveness but one of them (part c) seems to decrease the film cooling effectiveness by increasing the jet penetration. Among all of them, just part (b) depends on the upstream jet temperature and this flow parameter seems to have no effect on parts (a) and (c).

In order to elucidate the main reason for increases in film cooling effectiveness, the upstream cold jet was replaced with a hot one and its effects on span-wise averaged film cooling effectiveness was investigated as shown in Fig. 13. From this figure, it is evident that part (c) has major effects on improving the film cooling effectiveness in both near and far field of the jet. However, effects of part (a) and (c) strongly depend on the

upstream to main jet width ratio and increases as this ratio increases.

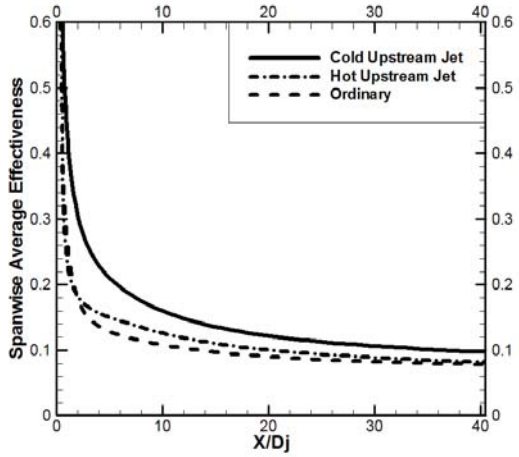

Figure 13. Comparison of span-wise film cooling effectiveness between hot and the cold upstream jets.

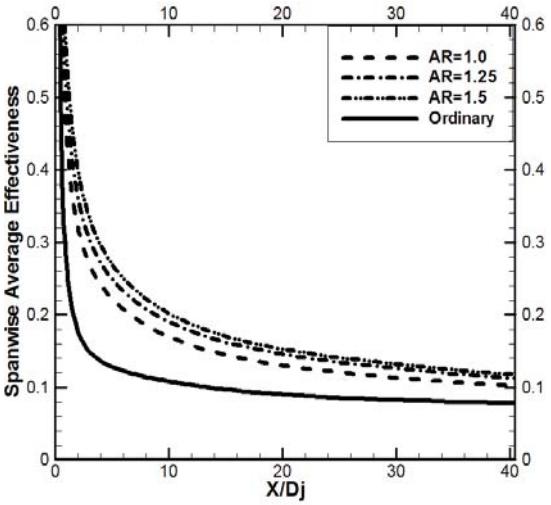

Figure 14. Span-wise averaged film cooling effectiveness plots for three different area ratios.

7.3 Effects of Jets' Area Ratio

In this section, effects of the upstream jet to the main jet area ratio on the flow hydrodynamics and adiabatic film cooling effectiveness are investigated. In this research, the X-direction width of the upstream jet was kept constant; hence, the area ratio can be defined as the ratio of the upstream jet Z-direction width to the main jet Z-direction width. That is,

$$\mathrm{AR} = \frac{The\ \ upstream\ \ jet\ \ Z-direction\ \ width}{The\ \ main\ \ jet\ \ Z-direction\ \ width}. \tag{26}$$

The simulations are performed for three different area ratios of 1.0, 1.25, and 1.5.

Figure 14 shows the span-wise averaged film cooling effectiveness plots for three different area ratios. From this figure, it is evident that higher effectiveness is related to higher area ratios. Similar trends are evident in Fig. 15 which gives the centerline film cooling effectiveness.

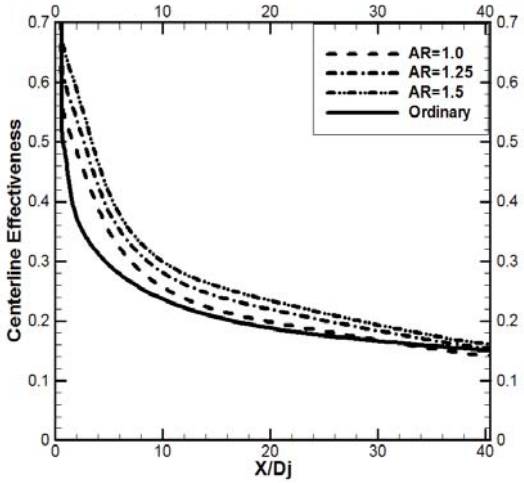

Figure 15. Centerline film cooling effectiveness plots for three different area ratios.

Figure 16 shows the rise in span-wise averaged effectiveness in comparison to that of the ordinary single jet for different area ratios. According to this figure, the rise in total averaged effectiveness is about %53 for AR=1.0, %73 for AR=1.25, and %84 for AR=1.5. By further increasing the area ratio, the total film cooling effectiveness also increases continuously. However, structural considerations dictate an upper bound for this ratio.

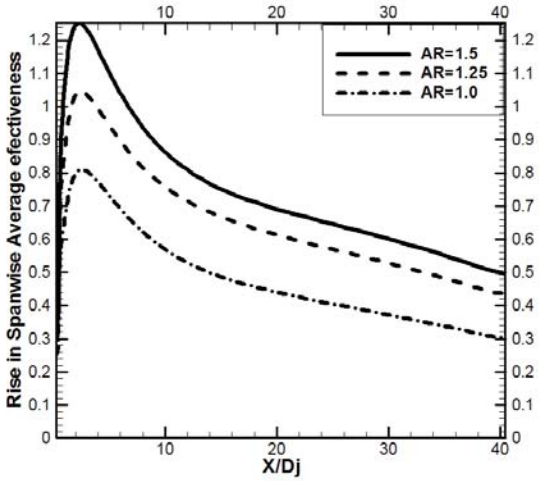

Figure 16. Rise in span-wise averaged effectiveness for three different area ratios.

7.4 Effects on the Skin Friction Drag

The skin friction drag is related to the stream-wise velocity gradient in the vicinity of the wall. Therefore, by using the film cooling approaches to protect the surface from thermal stresses, the velocity gradient and, hence, the skin friction drag reduces compared to that of the fully developed turbulence flow over a plate. Also, this reduces the aerodynamic losses in the turbine blades. Fig. 17 compares the centerline skin friction drag coefficients. As shown in this figure, the skin friction drag in the new configuration is about %200 lower than that of the ordinary cooling jet system.

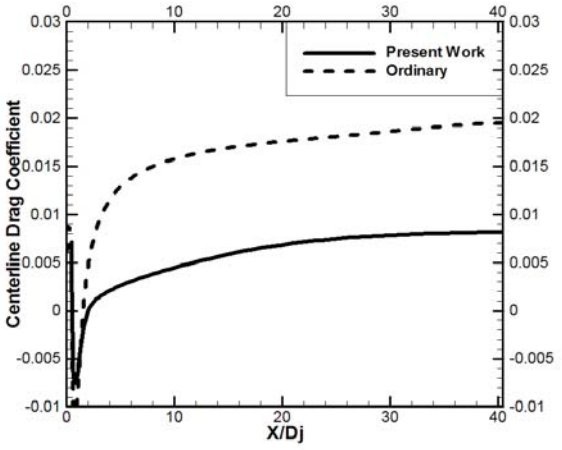

Figure 17. Comparison of the centerline skin friction drag coefficient for the new configuration and for the ordinary film cooling configuration.

8 Conclusions

In this research, it is proposed to improve the film cooling adiabatic effectiveness by introducing a new near-wall control technique. In this technique, a small injection port is used just upstream of the main jet. The obtained results showed that the upstream jet changes the flow pattern in such a way that the HSVs become much wider in the Z-direction. This allows the film cooling fluid to spread out more laterally and introduce more uniform coolant distribution over the surface. Also, when a cold upstream jet is applied, the coolant fluid of this upstream jet moves to fill the separation region beneath the main jet. This flow feature was found to improve the adiabatic effectiveness, especially in the near field of the cooling jet.

The effects of the upstream jet on the main jet area ratio are investigated, too. The obtained results showed an improvement in the span-wise averaged adiabatic effectiveness as the area ratio increases from 1.0 to 1.5. Also, the near field (X/ Dj <10) of the jet was more affected by changing the area ratio. However, this increase in the area ratio is limited by the structural capabilities of the turbine blades to withstand extra stresses due to wider upstream hole. Also, the skin friction drag was considerably reduced in the new configuration compared to that of the ordinary film-cooling configuration, especially when the area ratio increases. Finally, it should be noted that the adiabatic effectiveness could be increased even by applying a hot upstream jet.

9 References

1. Yuen, C.H.N. and Martinez-Botas, R.F. “Film Cooling Characteristics of a Single Round Hole at Various Streamwise Angles in a Crossflow: Part I Effectiveness”, *International Journal of Heat and Mass Transfer*, Vol. 46, No. 2, pp. 221-235, 2003.

2. Rozati, A. and Tafti., D.K., “Large-eddy Simulations of Leading Edge Film Cooling: Analysis of Flow Structures, Effectiveness, and Heat Transfer Coefficient”, *International Journal of Heat and Fluid Flow*, Vol. 29, No. 1, pp. 1-17, 2008.

3. Guo, X., Schroder, W., and Meinke, M., “Large Eddy Simulations of Film Cooling Flows”, Computers & Fluids, Vol. 35, No. 6, pp. 587–606, 2006.

4. Altorairi, M.S., “Film Cooling from Cylindrical Holes in Transverse Slots,” M.Sc. Thesis, Graduate Faculty of the Louisiana State University and Agricultural and Mechanical College, 2003.

5. Baheri, S., Alavi-Tabrizi, S.P., and Jubran, B.A., “Film Cooling Effectiveness from Trenched Shaped and Compound Holes,” *Heat and Mass Transfer. J.*, Vol. 44, No. 8, pp. 989-998, 2008.

6. Waye, S.K., and Bogard, D.G., "High-Resolution Film Cooling Effectiveness Measurements of Axial Holes Embedded in a Transverse Trench with Various Trench Configurations", *Journal of Turbomach.*, Vol. 129, No. 2, pp. 294-302, 2007.

7. Ramezanizadeh, M., Taeibi-Rahni, M., and Saidi, M.H., "Investigation of Density Ratio Effects on Normally Injected Cold Jets into a Hot Cross Flow", Arch. Appl. Mech., Vol. 77, No. 11, pp. 835-847, 2007.

8. Dittmar, J., Schulz, A., and Wittig, S., "Adiabatic Effectiveness and Heat Transfer Coefficient of Shaped Film Cooling Holes on a Scaled Guide Vane Pressure Side Model", *International Journal of Rotating Machinery*, Vol. 10, No. 5, pp. 345-354, 2004.

9. Miao, J. and Wu, C.Y., "Numerical Approach to Hole Shape Effect on Cooling Effectiveness over Flat Plate Including Internal Impingement Cooling Chamber," *International Journal of Heat and Mass Transfer*, Vol. 49, No's. 5-6, pp. 919-938, 2006.

10. Lu, Y., Allison, D., and Ekkad, S., "Turbine Blade Showerhead Film Cooling: Influence of Hole Angle and Shaping", *International Journal of Heat and Fluid Flow*, Vol. 28, No. 5, pp. 922-931, 2007.

11. Yuen, C. and Botas, R. M., "Film Cooling Characteristics of a Single Round Hole at Various Streamwise Angles in a Crossflow: Part I Effectiveness", *International Journal of Heat and Mass Transfer*, Vol. 46, No. 2, pp. 221-235, 2003.

12. Goldestein, R.J., Jin, P., and Oslo, R.L., "Film Cooling Effectiveness and Mass/Heat Transfer Coefficient Downstream of One Row of Discrete Hole Film Cooling", *Journal of Turbomachinery*, Vol. 121, No. 4, pp.225-232, 1999.

13. Rowbury, D.A., Oldfield, M.L.G., and Lock, G.D., "A Method For Correlating the Influence of External Crossflow on the Discharged Coefficient of Film Cooling Holes", *Journal of Turbomachinery*, Vol. 123, No. 2, pp. 258-265, 2001.

14. Cutbirth, J.M. and Bogard, D.G., "Evaluation of Pressure Side Film Cooling with Flow and Thermal Field Measurements, Part 2: High Meanstream Turbulence", *Journal of Turbomachinery*, Vol. 124, No. 4, pp. 678-685, 2002.

15. Sangkwon, N. and Shih, T., "Increase Adiabatic Film-Cooling Effectiveness by Using an Upstream Ramp", *Journal of Heat Transfer*, Vol. 129, No. 4, pp. 464-471, 2006.

16. Javadi, Kh., Taeibi-Rahni, M., Darbandi, M., "Jet-into-Crossflow Boundary-Layer Control: Innovation in Gas Turbine Cooling", *AIAA Journal*, Vol. 45, No. 12, pp 2910-2925, 2007.

17. Acharya, S., Tyagi, M., and Hoda, A., "Flow and Heat Transfer Prediction for Film Cooling Heat Transfer in Gas Turbine System", Annals of the New York Academy of Science, 934, pp. 1-9, 2001.

18. Jones, R. M., "Advance Turbulence Modeling for Industrial Flow", Ph.D. Dissertation, Louisiana State University, Baton Rouge, Louisiana, 2003.

19. Jones, R.M., Acharya, S., and Harvey, A., "Modeling and Simulation of Turbulent Heat Transfer", 1st Ed., Witt Press, New York, 2005.

20. Ajersch, P., Zhou, J. M., Ketler, S., Salcudean, M., and Gartshore, I.S., "Multiple Jets in a Crossflow: Detailed Measurements and Numerical Simulation", Int. Gas Turbine and Aeroengine Congress and Exposition, ASME Paper 95-GT-9, Houston, TX, pp. 1-16, 1995.

21. Davidson, L., "An Introduction to Turbulence Models", Department of Thermo and Fluid Dynamics, Chalmers University of Tecnology, 2003.